J Mater Sci: Mater Electron (2015) 26:590–600
DOI 10.1007/s10854-014-2440-y

Highly electrically conductive adhesives using silver nanoparticle (Ag NP)-decorated graphene: the effect of NPs sintering on the electrical conductivity improvement

Behnam Meschi Amoli · Josh Trinidad · Anming Hu · Y. Norman Zhou · Boxin Zhao

Received: 27 August 2014 / Accepted: 23 October 2014 / Published online: 4 November 2014

Abstract Electrically conductive adhesives (ECAs) filled with silver nanoparticle (Ag NP)-decorated graphene were prepared and the effect of curing temperature on the electrical conductivity of the ECAs was discussed. Mono-dispersed Ag NPs with an average size of 9 nm were successfully deposited and simultaneously functionalized with mercaptopropionic acid (MPA) on graphene surface. The surface functionalization of the NPs with MPA made the decorated graphene dispersible in organic solvents, which facilitated its dispersion inside epoxy. The decorated graphene was added into conventional ECAs (consisting of silver flakes and epoxy) at concentrations close to the percolation threshold and beyond that resulting in a significant electrical conductivity improvement (especially at concentrations close to the percolation threshold). The electrical resistivity of hybrid ECAs with the decorated graphene decreased as the curing temperature increased. Curing the ECA with 1 wt% of the decorated graphene at 220 °C resulted in a highly conductive adhesive with a low electrical resistivity of 4.6×10^{-5} Ω cm (close to that of eutectic lead based solders). The dramatic electrical conductivity improvement of ECAs is due to the sintering between small Ag NPs on the graphene surface and silver flakes. Morphological and thermal studies showed that Ag NPs start to sinter at approximately 150 °C when the MPA layer began to decompose from their surface. The quality of filler–filler interaction was investigated by monitoring the effect of temperature on the electrical resistivity of conductive fillers "thin-film" before their addition to epoxy.

B. Meschi Amoli · J. Trinidad · B. Zhao (✉)
Department of Chemical Engineering, University of Waterloo, 200 University Avenue West, Waterloo, ON N2L 3G1, Canada
e-mail: zhaob@uwaterloo.ca

B. Meschi Amoli · J. Trinidad · Y. N. Zhou · B. Zhao
Waterloo Institute for Nanotechnology, University of Waterloo, 200 University Avenue West, Waterloo, ON N2L 3G1, Canada

B. Meschi Amoli · A. Hu · Y. N. Zhou · B. Zhao
Centre for Advanced Materials Joining, University of Waterloo, 200 University Avenue West, Waterloo, ON N2L 3G1, Canada

A. Hu · Y. N. Zhou
Department of Mechanical and Mechatronics Engineering, University of Waterloo, 200 University Avenue West, Waterloo, ON N2L 3G1, Canada

A. Hu
Department of Mechanical, Aerospace and Biomedical Engineering, University of Tennessee Knoxville, 509 Doughty Engineering Building, 1512 Middle Drive, Knoxville, TN 37996-2210, USA

1 Introduction

In recent years, a substantial amount of research has been carried out on the fabrication of polymer nanocomposites reinforced by metallic fillers. These nanocomposites have been used to develop new types of electrically conductive adhesives (ECAs) as promising alternatives for traditionally used lead-based or lead free solders in electronic packaging industries. Along with their light weight and low environmental impact, ECAs offer many other advantages over traditional solders, including milder operating conditions, fewer processing steps, reduced thermo-mechanical residual stress on the substrate, and finer-pitch capability [1, 2].

As the next generation of interconnecting materials for today's large and growing advanced electronic industry, ECAs are required to maintain high electrical conductivity while providing additional benefits. The conventional ECAs, consisting of thermoset polymers (e.g., epoxy) and silver micro flakes, render higher electrical resistivity

(10^{-3}–10^{-4} Ω cm) than eutectic lead-based solders (2×10^{-5} Ω cm) even at high silver contents [3]. The low electrical conductivity of conventional ECAs is due to the inability of silver flakes to provide metallurgical connections within the electrical network as eutectic solders do [4]; this situation limits ECAs to the applications that only can tolerate low electrical conductivity. The incorporation of nano-sized silver particles into the conventional formulation of ECAs has been proposed to improve the electrical conductivity of ECAs and broaden their application. It has been reported that spherical Ag NPs can be melted at temperatures far less than their bulk melting point (due to the depressed melting point effect) and provide metallurgical connection between silver flakes [5–7]. One dimensional (1-D) silver nanostructures [e.g., nanowires (NWs), nanobelts (NBs), etc.] were found to be more effective than spherical NPs at enhancing the electrical conductivity of ECAs. The 1-D nanostructures can provide more electrical pathways inside ECAs and establish a percolated network at lower filler contents while still taking advantage of the depressed melting point effect due to their nano size [8–10].

Since their discovery, graphene nanosheets have drawn an intensive attention towards a variety of research fields to utilize their exceptional thermal, mechanical, optical and electrical properties. These nanosheets are flat monolayers of carbon atoms, 0.335 nm thick, densely packed into a honeycomb 2-D lattice structure [11–13]. Possessing the largest aspect-ratio among all the nano-structured materials and also having 2-D structure, graphene nanosheets are promising nanomaterials able to establish a percolated network at very low concentrations. Luan et al. [14], demonstrated the significant potential of graphene to reduce the percolation threshold of ECA by decreasing the tunneling resistance in the electrical network. However, one challenge with the use of graphene is its aggregation during mixing with polymers, as graphene nanosheets tends to attract one another with strong van der Waals forces [15, 16]. In order to harness the characteristic properties of graphene, the nanosheets need to preserve their unique single layer structure [17]. Pasricha et al. [18] reported that the decoration of graphene with Ag NPs is an effective way to exfoliate graphene nanosheets, and to prevent their aggregation. Apart from the aggregation problem, the quality of filler–filler contact is another important issue, as the contact resistance between graphene and silver flakes is higher than that of two silver species [10, 19]. Oh et al. [10], reported a significant contact resistance reduction when they decorated carbon nanotubes (CNTs) with glutaric acid-functionalized Ag NPs. Considering the higher aspect ratio of graphene than CNTs [20], the Ag NP-decorated graphene should be more promising nanofiller to improve the electrical conductivity of conventional ECAs as Peng et al. [21], recently reported the electrical conductivity improvement of ECAs via addition of Ag NP-decorated graphene to the conventional ECAs. If Sintering of Ag NPs on the graphene surface occurs, it can significantly decrease the contact resistance between neighboring fillers via the formation of metallurgical contacts between silver flakes and graphene nanosheets. It should be noted that the organic layer over the surface of the Ag NPs has an important impact on their sintering behavior [5, 8]. The smaller amount of organic material and the shorter organic chain length help the sintering at low temperature, as well as electron transferring inside the network [5–7]. Recently, Liu's research group developed new in situ approaches to decorate the graphene surface with Ag NPs for ECAs application [19, 22]. In their method, the formation of Ag NPs on graphene surface occurs during the curing process of epoxy, making the NPs size very sensitive to curing temperature. Although in situ approaches eliminate the use of organic layer over NPs surface, it makes it difficult to keep the NPs size constant as the curing temperature changes. Furthermore, at temperatures less than NPs formation temperature, there would be no Ag NPs inside the nanocomposites, thereby limiting the applications of the ECAs to those operating at temperatures higher than NPs formation temperature.

In this article, we employed a simple wet chemistry approach to decorate the graphene surface with Ag NPs for electrically conductive adhesive applications and carried out a systematic investigation on the effect of NPs sintering on the electrical conductivity improvement of hybrid ECAs. The NPs were functionalized with mercaptopropionic acid (MPA) to control their size and to prevent their oxidation. The small size of the NPs covered by very short chain length organic layer (MPA with 3 carbon atoms chain length) makes the NPs dispersible in organic solvent and possible to sinter at low temperatures. By decorating the graphene surface with small size MPA-functionalized Ag NPs and introducing them into epoxy/silver composite, we can provide metallurgical connection between neighboring fillers at low temperatures and also increase the surface area for electron transportation inside the electrical network. The electrical conductivity of the hybrid ECAs were measured at different curing temperatures and compared to those of conventional ECAs and hybrid ECAs with non modified graphene. The mechanism of electrical conductivity improvement was discussed according to the quality of filler–filler interaction at different temperatures. The sintering behavior of conductive fillers was investigated using morphological, electrical, and thermal studies. A highly conductive hybrid ECA was prepared by introducing a small amount of Ag NP-decorated graphene nanosheets (1 wt%) to the conventional formulation of ECAs. The resultant hybrid ECAs was found to have a bulk

resistivity of 4.6×10^{-5} Ω cm which is close to that of lead-based solders [3].

2 Experiments and methods

2.1 The decoration of graphene with MPA-functionalized Ag NPs

Graphene oxide (GrO) was first prepared before the deposition of Ag NPs. For this, 50 mg of graphene nanosheets (ACS material, USA) with an average size of 1 μm was dispersed into a solution of sulfuric and nitric acids (3:1 volume ratio) and stirred at 70 °C for 20 min. The solution was then filtered using a polycarbonate (PC) membrane (with a pore size of 100 nm) and washed several times with de-ionized (DI) water until the pH became neutral. The filtrate was dried in a vacuum oven overnight.

The deposition of Ag NPs on the surface of graphene oxide nanosheets is based on the direct reduction of Ag ions (adsorbed on the surface of graphene oxide) using a strong reducing agent ($NaBH_4$) in the presence of MPA. First, 20 mg of GrO was dispersed in 50 mL DI water using a bath sonicator for 30 min. Second, a solution of 170 mg $AgNO_3$ (≥99 wt%, Sigma-Aldrich) in THF and DI water (5:1 volume ratio) was added to GrO solution and stirred for 1 h. Third, a 20 mL solution of MPA (≥99 wt%, Sigma-Aldrich) in THF was added to the mixture in a drop wise fashion. Finally, 10 mL aqueous solution of $NaBH_4$ (≥99 wt%, Sigma-Aldrich) was added to the mixture, leading to an abrupt precipitation of a dark solid. To remove the un-attached Ag NPs from system, the mixture was filtered using a PC membrane (with a pore size of 400 nm) and continuously washed with DI water.

2.2 Preparation of conductive filler "thin-films"

To prepare a "thin-film" of silver flakes and Ag NP-decorated graphene for "thin-film" conductivity measurements, the decorated graphene was dispersed into 5 mL of ethanol using a bath sonicator for 30 min. 100 mg of silver flakes (Aldrich, 10 μm) was then added; and, the solution was sonicated for 30 min. The solution was then deposited on a glass slide and heated at different temperatures for 1 h to evaporate the solvent. The same procedure was performed to prepare pure silver flake "thin-film" as well as silver flakes and non-modified graphene "thin-film".

2.3 Nanocomposite preparation

The Ag NP-decorated graphene along with silver flakes were added to epoxy (diglycidyl ether of bisphenol A, DERTM 322, DOW chemical company, USA). To ensure a good dispersion of the decorated graphene in the viscous epoxy, the decorated graphene was first dispersed into ethanol for 30 min using a bath sonicator. Ag flakes and epoxy were then added to the decorated graphene dispersion; the mixture was further mixed using a vortex mixer for 20 min followed by ultrasonication for 1 h. The mixture was then degassed under vacuum for 1.5 h to remove the solvent from the system. After degassing, the curing agent, triethylenetetramine (TETA, DOW chemical company, USA), was added to the mixture. The weight ratio of the curing agent to epoxy was 0.13. The final mixture was filled into a mold of $7 \times 7 \times 0.5$ mm^3 (L × W × D) made on a pre-cleaned microscope glass slide using pieces of adhesive tape. To fabricate a smooth surface and control the sample thickness, a clean copper plate was placed on top of the mold; the extra material was squeezed out. The samples were pre-cured for 30 min at 60 °C and then post cured at different curing temperatures (i.e., 150, 190, and 220 °C) for 2 h. After curing, the copper plate and adhesive tape were peeled off. Similar mixing and curing procedures were applied to prepare hybrid ECAs with non-modified graphene and conventional ECAs except that for conventional ECA there was no graphene in the system. It should be noted that in hybrid ECAs, the weight fraction of both modified and non-modified graphene was kept at 1 wt%.

2.4 Characterization methods

Fourier transform infrared spectroscopy (FTIR) (Tensor 27, Bruker Co.) was performed to verify the functionalization of Ag NPs on the surface of graphene nanosheets. A high resolution transmission electron microscope (HRTEM, JEOL 2010 F FEG), operated at 200 kV and equipped with Gatan ultra scan imaging filter, was used to characterize the size of Ag NPs on graphene surface. The morphologies of the decorated graphene and conductive "thin-films" were examined by scanning electron microscope (SEM, LEO FE-SEM 1530, Carl Zeiss NTS) operated at 10 kV. Ultraviolet–Visible spectroscopy (UV–Vis) (UV-2501 pc, Shimadzu) was performed to confirm both the synthesis and the quality of size distribution of the synthesized Ag NPs on the graphene surface. X-ray diffraction (XRD) patterns of the decorated graphene were collected on a D8 Discover Bruker instrument equipped with Cu-Kα radiation. To collect the XRD patterns, samples were deposited on a glass sample holder. The weight-loss of Ag NPs and the decorated graphene were studied using thermogravimetric analysis (TGA, TA instrument, Q500-1254). A sample of approximately 3 mg was placed into the TGA sample pan, and a dynamic scan was performed from 40 to 800 °C with a heating rate of 10 °C/min under a 50 mL/min nitrogen purge atmosphere. The sheet resistance of

samples was measured using a four-point probe setup consisting of a probe fixture (Cascade microtech Inc.) and a source meter (Keithley 2440 5A Source Meter, Keithley Instruments Inc.). The sheet resistance was converted to the bulk resistivity according to:

$$\rho = F.t\frac{\pi}{\ln 2}\left(\frac{V}{I}\right) \quad (1)$$

where t is samples thickness, I is the applied current, and V is the voltage drop measured by the source meter. In Eq. 1, F is a correction factor for a finite sample with finite thickness. F is a function of the ratio of sample thickness (t) to probe spacing (s). For $0.4 < \frac{t}{s} < 1$, F is close to 1. In our system, in which the samples thickness is 0.5 mm and the probe spacing is 1 mm, F can be safely considered as 1.

3 Results and discussion

3.1 Ag NP decoration of graphene nanosheets

The schematic mechanism of Ag NP decoration of graphene is illustrated in Scheme 1. In order to decorate graphene with Ag NP, the graphene nanosheets were first oxidized to generate polar functional groups (hydroxyl and carboxylic groups) on their surface (shown in Scheme 1a) using a typical acid treatment process with a mixture of sulfuric and nitric acids (3:1 volume ratio). The resulted GrO was dispersible in water, which is needed for further surface modification as the synthesis of Ag NPs on the graphene surface is performed in an aqueous medium. Comparing the FTIR spectra of the non-modified graphene and GrO (Fig. 1a) confirms the presence of polar functional groups on acid-treated graphene surface. The peak at 1,704 cm^{-1} is attributed to the C=O carbonyl stretching vibrations of carboxylic groups, while this peak is damped before acid treatment [23]. The strong and broad peak around 3,400 cm^{-1} is assigned to O–H stretching vibrations due to hydroxyl groups of GrO [18]. In addition, the peaks at 1,617, and 1,228 cm^{-1} in the GrO spectrum are attributed to the C=C stretching and C–OH stretching bands, respectively [24]. Similar peaks with a slight shift are observed in the spectrum of the non-modified graphene. The FTIR results confirm that the graphene is successfully functionalized with hydroxyl and carboxylic groups through the acid treatment process. The functionalization can be further verified by comparing the dispersion qualities of graphene in polar solvents, i.e., ethanol and water, before and after acid treatment. Graphene before the treatment was not dispersible in ethanol and water while the GrO was dispersible and stable in both solutions for more than 8 h (see Fig. 1b).

Ag NPs were synthesized on GrO surface through a two-step process as illustrated in Scheme 1b, c. In the first step,

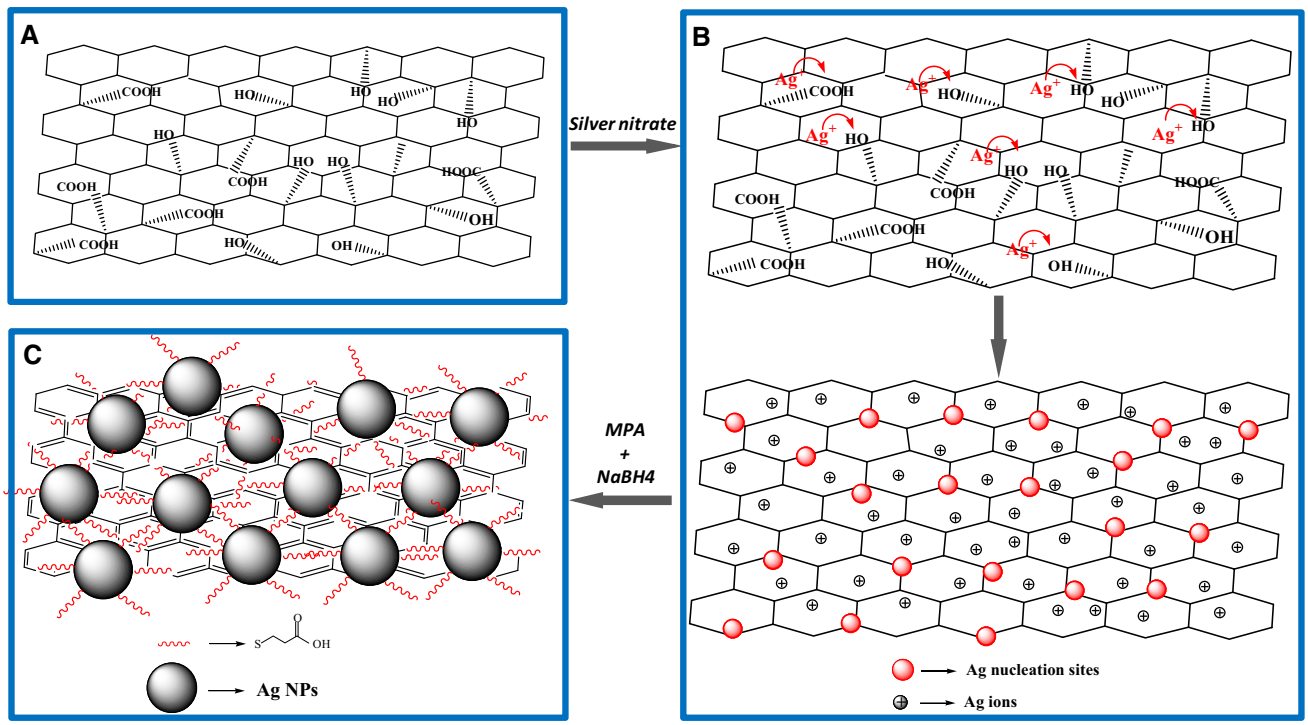

Scheme 1 A schematic of silver decoration over the surface of graphene; **a** GrO with oxygen functionalities, **b** adsorption of Ag ions on the oxygen functionalities of the graphene surface to form nucleation sites for Ag NPs, **c** graphene decorated with MPA-functionalized Ag NPs

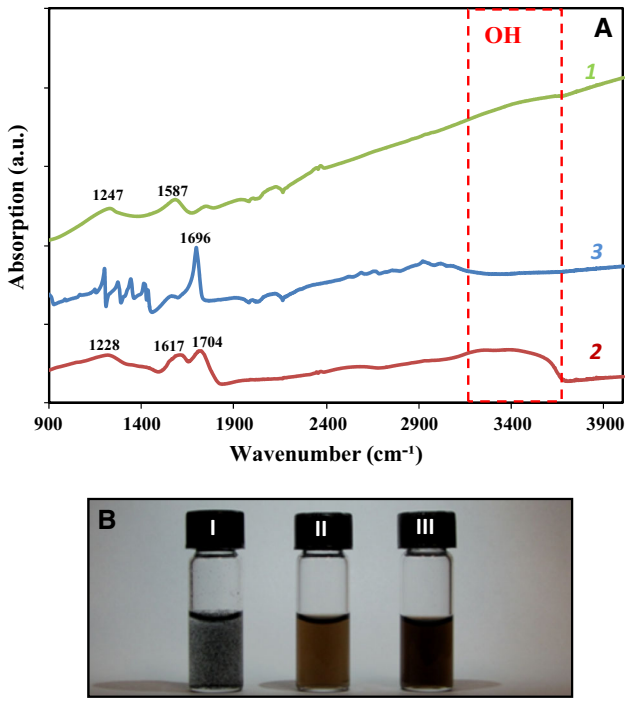

Fig. 1 **a** The infrared spectrum of non-modified graphene (*curve 1*), GrO (*curve 2*) and Ag NP-decorated graphene (*curve 3*); **b** digital images of the dispersion of (*I*) non-modified graphene, (*II*) GrO, and (*III*) Ag NP-decorated graphene in ethanol

GrO and $AgNO_3$ aqueous solutions were stirred together for 1 h to provide initial active nucleation sites on the surface of graphene. The carboxylic groups, uniformly distributed on the graphene surface [25], form a complex with the Ag ions and attach them to the surface of graphene [18]. The reduction of Ag ions on GrO surface has been reported in recent literature [18, 23, 25]. Although the role of oxygen functionalities of GrO in reducing Ag ions is well accepted, it is not fully understood which type of these oxygen moieties is responsible for the reduction of these ions. The reducing nature of GrO might be a result of the presence of hydroxyl groups on hexagonal basal planes, providing phenolic entities on the graphene surface. Phenolic protons are weak acids and can be deprotonated to form active phenolate anions. These anions donate one electron to the Ag ions, reducing them to Ag^0 [18]. Ag NPs, formed during this step, may also interact with the graphene surface through physisorption, electrostatic binding, or through a charge-transfer interaction [18, 24]. Figure 2a shows a representative SEM image of graphene oxide nanosheets before decoration. Figure 2b shows the Ag NPs formed in the first step on the graphene surface. As can be observed in this figure, very small NPs are homogeneously distributed on the graphene surface which is related to the uniform distribution of oxygen functionalities over GrO surface. As can be seen in Fig. 2c there is no agglomeration of Ag NPs on the surface of graphene. The size of individual NPs, formed in this step, is <5 nm. Figure 2d shows the EDX spectrum of the elemental state of Ag NPs on graphene surface (i.e. first step of Ag NP decoration of graphene). A relatively strong peak of Ag (pointed by the black arrow) in this spectrum along with the peaks of carbon and oxygen confirms the formation of Ag NPs in this stage. The presence of the oxygen peak implies oxygen functionalities still exist on the graphene surface.

The second step of Ag NP decoration of graphene is based on the direct reduction of the remaining Ag ions by $NaBH_4$ in the presence of MPA as a capping agent. MPA chains, with a sulfur group at one end and a carboxylic group at the other, form micellar structures at the nucleation sites in THF/water medium and trap the remaining Ag ions [6]. When MPA was added to the solution of GrO and $AgNO_3$, the initial dark solution became greyish along with the formation of small clusters in the solution. In our previous paper, we found that the color change is associated with the formation of Ag–S bands [6, 26]. Upon the addition of $NaBH_4$, all the ions are reduced to Ag^0 and form Ag NPs covered by MPA on the graphene surface. The role of MPA is to control the size and shape of NPs and to prevent them from oxidization [6]. As shown in Fig. 1a, the strong and sharp peak at 1,696 cm^{-1} in the FTIR spectrum of the Ag NP-decorated graphene is attributed to the carbonyl stretching frequency resulting from the semiquinone moieties on Ag NPs surface [18]. The surface MPA of Ag NPs makes the decorated graphene dispersible in polar solvents (i.e., ethanol and water); Fig. 1b (sample 3) shows a stable dispersion of the Ag NP-decorated graphene in ethanol. The same quality of stability was observed for the decorated graphene in water.

Apart from reducing Ag ions, $NaBH_4$ plays an important role in restoring the conjugated sp^2 network. Some research groups reported the contribution of $NaBH_4$ in reducing GrO to graphene and increasing its conductivity [27, 28]. The diminished spectra of Fig. 1a at 3,400 cm^{-1} for Ag NP-decorated graphene implies there is no oxygen moiety on the surface of graphene after the completion of the decoration of graphene, which in turn confirms the restoration of π–π carbon bonds after the decoration of the graphene surface.

UV–Vis spectroscopy was performed to confirm the synthesis of the individual Ag NPs on the graphene surface. It is well known that Ag NPs larger than 2 nm show a strong and broad peak in the UV–Visible range (390–460 nm) due to the excitation of surface plasmon bonds (SPB) [29]. The position and symmetrical feature of this peak give useful information about both the size and size distribution of the NPs. Figure 3a shows the UV–Vis spectra of GrO, Ag NP-decorated graphene, and the

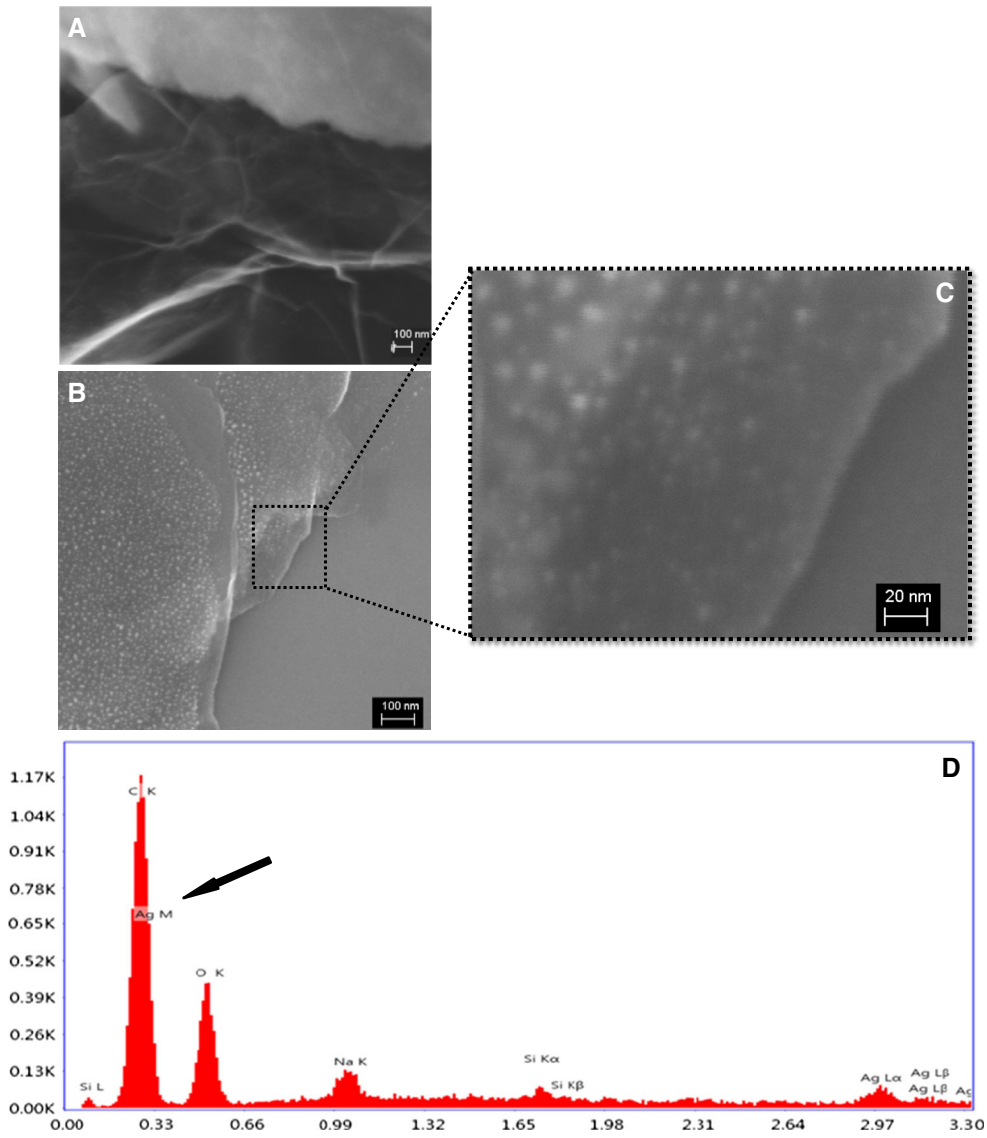

Fig. 2 **a** A representative SEM image of GrO before decoration. **b** A representative SEM image of silver nucleation on the graphene surface; **c** a magnified image of the selected area of **b**; **d** EDX diagram of the elemental state of Ag NPs on the surface of graphene (the *black arrow* indicates the relative strong peak of Ag)

individual Ag NPs fabricated with a similar procedure [6]. The UV–Vis spectrum of GrO shows a peak around 223 nm corresponding to $\pi \rightarrow \pi^*$ transitions of aromatic C–C bonds [24]. For the Ag NP-decorated graphene, the presence of the characteristic peak at 394 nm clearly indicates the formation of Ag NPs on the graphene surface. The symmetry of this peak implies a homogeneous size distribution of the NPs. Compared to the spectrum of the individual Ag NPs, the spectrum of the Ag NP-decorated graphene shows a shoulder at 270 nm which is attributed to graphene aromatic C–C bonds. The presence of this peak further confirms the decoration of graphene with Ag NPs. The XRD pattern of the Ag NP-decorated graphene is shown in Fig. 3b. The dominant peaks are observed at 38.2°, 44.3°, 64.6°, and 77.6° with corresponding to 2θ values. According to JCPDS card No. 07-083, these peaks correspond to the (1 1 1), (2 0 0), (2 2 0) and (3 1 1) crystallographic planes of face center cubic (fcc) of the Ag NPs. The highest diffraction intensity is found for the peak at 38.2°, which indicates that the surface of Ag NPs is preliminary (1 1 1) planes that are considered the most stable crystalline structure [30]. Graphene nanosheets usually show a diffraction peak at 26° which corresponds to the 0.335 nm interlayer spacing of graphite [31]. In the diffraction pattern of GrO, another peak is observed at 13.6°, suggesting possible partial structural damage of graphene after oxidation. Others have observed similar trends in the shift of the XRD peak to lower angles due to the chemical oxidation of graphene [32, 33]. However, this peak has been dampened and shifted to 12.2° indicating the effectiveness of $NaBH_4$ in restoring the conjugated sp^2 bands of graphene aromatic structure.

Figure 4a shows a TEM image of graphene sheets before treatment. A representative TEM image of the Ag

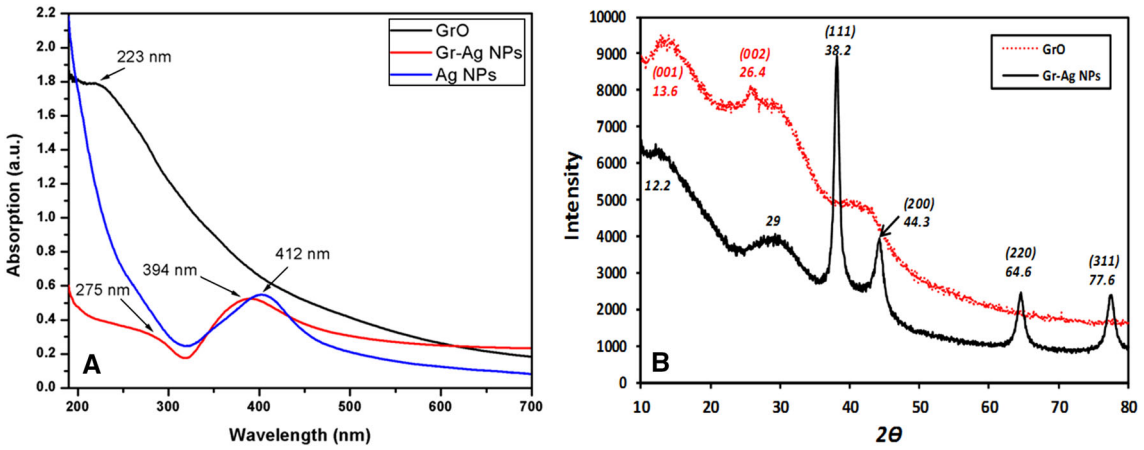

Fig. 3 **a** UV–Vis spectra of GrO, individual Ag NPs (synthesized with the same procedure as the Ag NPs on graphene surface), and Ag NP-decorated graphene; **b** XRD pattern of GrO and the Ag NP-decorated graphene

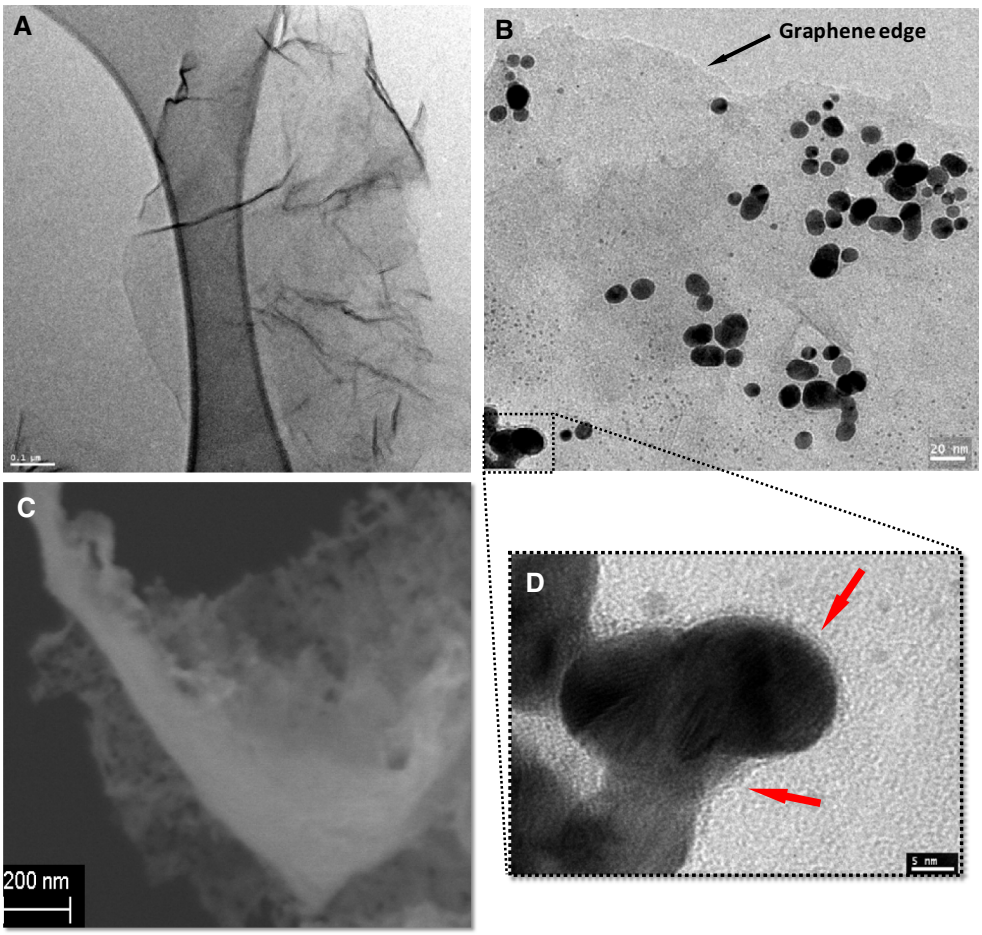

Fig. 4 **a** A representative TEM image of non-modified graphene; **b** a representative TEM image of the decorated graphene with MPA-functionalized Ag NP, the edge of graphene single layer are pointed by a *black arrow*; **c** a representative SEM image of the decorated graphene; **d** a HRTEM images of the selected area of **b**, showing the presence of an amorphous structure (pointed by *arrows*) of MPA on Ag NPs surface

NP-decorated graphene can be seen in Fig. 4b where the black arrow indicates to the graphene edge. As observed in this image, spherical Ag NPs with an average size of 9.1 ± 3.1 nm formed on the graphene surface along with some small particles (<2 nm). The small NPs are those formed in the first step and did not grow further. This image confirms that graphene maintained its smooth and very thin structure. Figure 4c displays a SEM image of the Ag NP-decorated graphene showing two layers of the decorated graphene beside one another. Figure 4d shows a

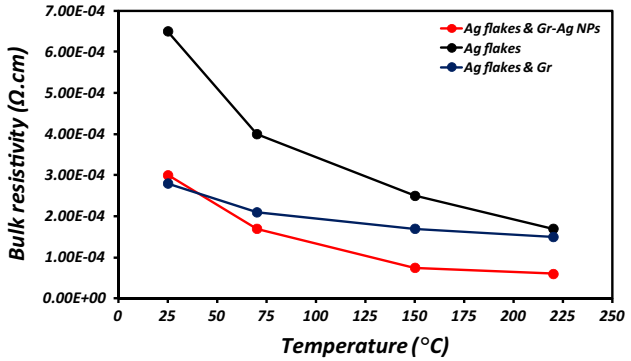

Fig. 5 The effect of temperature on the electrical conductivity of conductive fillers "thin-films" before their addition into epoxy

HRTEM image of the selected area of Fig. 4b. The amorphous structure over the surface of the NPs (as indicated by red arrows) clearly shows the surface coverage of Ag NPs by MPA. This image supports the FTIR results.

3.2 Electrical conductivity measurements of conductive filler "thin films" and nanocomposites

To investigate the effectiveness of the Ag NP-decorated graphene as a co-filler inside the electrical network, we first performed "thin-film" conductivity studies to examine the inter-filler interaction prior to adding them into epoxy matrix. The electrical resistivity of a "thin-film" of silver flakes and the decorated graphene as a novel hybrid filler system was measured and compared to those of pure silver flakes and silver flakes with non-modified graphene "thin-films" at varied temperatures. In each sample the total amount of silver was constant. The results are shown in Fig. 5. The electrical resistivity of hybrid filler system with both the decorated graphene (Ag flakes and Gr-Ag NPs) and non-modified graphene (Ag flakes and Gr) were decreased over the pure silver flake films (Ag flakes) for all measured temperatures. Due to its 2-D structure and high aspect-ratio, graphene provides more surface area for electron transportation inside the network and displays improved electrical conductivity with the hybrid filler system [14, 19].

As can be observed in Fig. 5, the electrical resistivity of all three film samples decreased as the temperature increased. However, the electrical conductivity improvement for hybrid filler film with the decorated graphene was more significant at higher temperatures than the other two. The increase in the electrical conductivity of both the pure silver flakes film and the hybrid filler films with non-modified graphene at higher temperature can be attributed to the increased packing density of silver flakes that enhanced the connection between conductive fillers. The significant improvements of the electrical conductivity for the hybrid filler film with the decorated graphene at higher temperatures (i.e., 150 and 220 °C) can be related to the contribution of the Ag NPs in the system. The presence of small Ag NPs on the graphene surface provides an opportunity to take advantage of the "melting depression effect". At higher temperatures, some Ag NPs began to sinter to each other as well as to the silver flakes. This situation provides metallurgical contacts between silver flakes and graphene which facilitates electron transportation throughout the electrical network.

Sintering of Ag NPs is largely affected by the amount of organic layer present on their surface and also by the temperature at which this layer is decomposed from the surface [7]. Thus, the thermal behaviour of the Ag NP-decorated graphene was studied using TGA to evaluate the phase transition of the Ag NPs on the graphene surface. Figure 6a shows the TGA results for Ag NPs and Ag NP-decorated graphene. For the individual Ag NPs, thermal decomposition began at 130 °C. The weight of the NPs decreased by 3 wt% until 285 °C due to the decomposition of un-bonded MPA and/or absorbed water in the system [6]. As the temperature increased, the NPs displayed two main thermal decomposition steps. The first transition occurred between 290 and 380 °C, displaying an approximate weight-loss of 8 wt% that may be attributed to the amount of MPA physisorbed on the surface of Ag NPs. The second transition with a 10 wt% weight-loss was observed at 385 °C, and continued up to 455 °C. This large weight-loss is attributed to the decomposition of chemisorbed organic materials [34]. Conversely, the thermal decomposition of surface residue for the Ag NP-decorated graphene occurs with a slight transition step, starting from 145 °C and ending at 375 °C, which can be attributed to the thermal decomposition of MPA adsorbed on the surface of the Ag NPs [6]. Comparing the TGA results of the decorated graphene with individual NPs indicates the thermal decomposition of MPA from the NPs surface occurs at lower temperature for the decorated graphene than individual NPs. These results also show a lower amount of MPA (<3.5 % for the Ag NP-decorated graphene compared to 22 % for the individual Ag NPs) covering the surface of the Ag NPs on the graphene surface, which helps with occurrence of sintering at lower temperature. TGA results suggested that at temperatures higher than 145 °C, Ag NPs on the surface of graphene started to sinter to each other.

The sintering of the NPs on the surface of graphene was further confirmed using SEM. Figure 6b shows an SEM image of a "thin-film" of Ag NP-decorated graphene and silver flakes mixture at room temperature. An SEM image of silver flakes "thin-film" at 220 °C is shown in Fig. 6c.

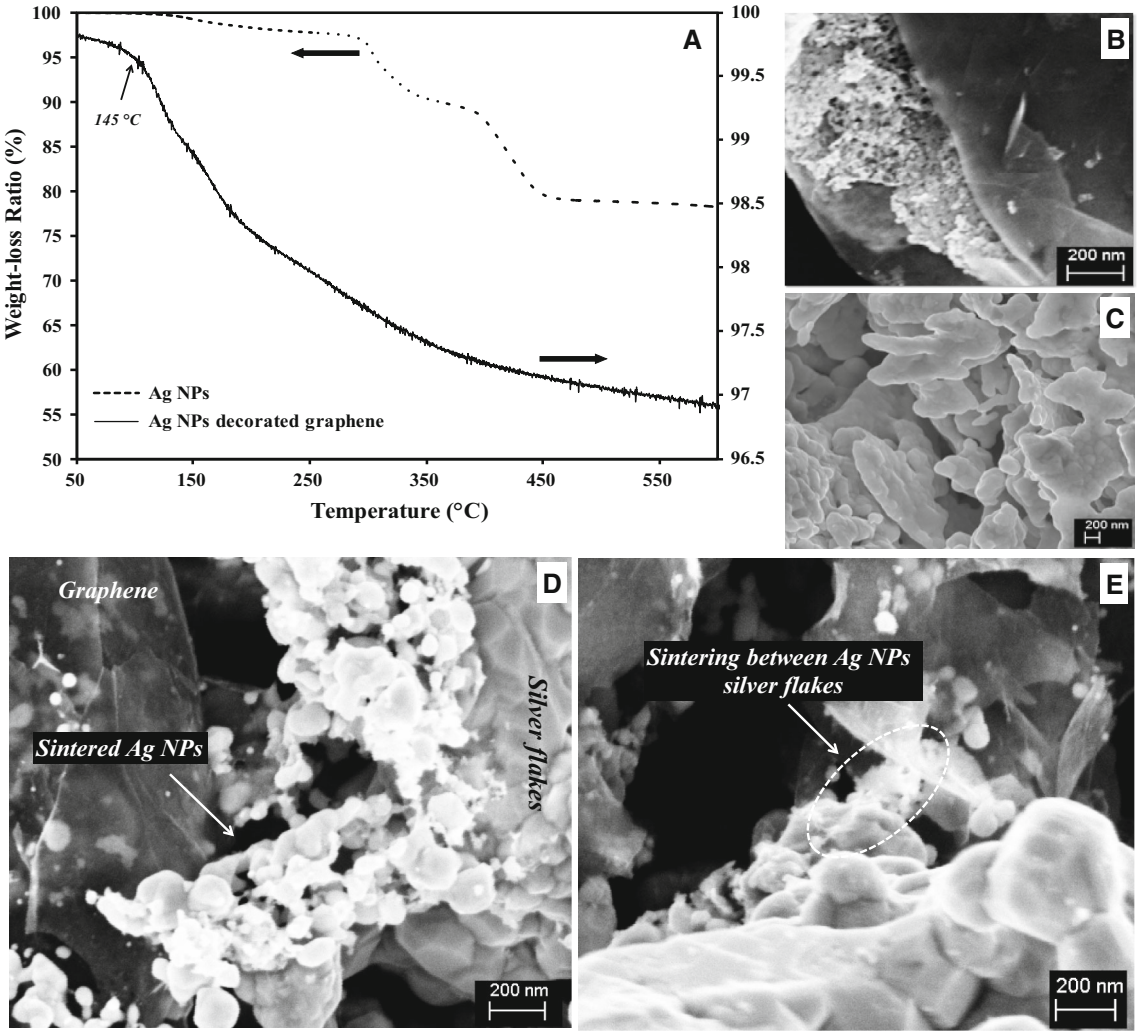

Fig. 6 **a** TGA analysis of the Ag NP-decorated graphene and the individual Ag NPs synthesized with the same procedure; **b** an SEM image of the "thin-film" of the Ag NP-decorated graphene and silver flakes mixture at room temperature; **c** SEM image of silver flakes "thin-film" at 220 °C; **d**, **e** SEM images of the Ag NP-decorated graphene and silver flakes "thin-films" at 150, and 220 °C, respectively, showing the sintering between the Ag NPs and flakes

Figure 6d, e show the SEM images of a "thin-film" of Ag NP-decorated graphene and silver flakes mixture at 150, and 220 °C, respectively. Comparison between the morphologies of the NPs in each case shows that sintering occurred between the NPs for the both samples annealed at 150, and 220 °C where they became whitish due to the removal of the organic layer from the surface [5]. In contrast, the NPs at room temperature did not sinter to each other, and instead had a dark color. Figure 6d, e also indicate the formation of metallurgical connections between the silver flakes and the decorated graphene, which can significantly improve the conductivity of the electrical network.

Hybrid ECAs were fabricated by adding a small amount of the Ag NP-decorated graphene (1 wt%) to the conventional ECAs consisting of silver micron flakes and epoxy. The decorated graphene was incorporated into conventional ECAs at two different silver contents, i.e., within and after the percolation threshold (60 and 80 wt%, respectively) and the final composites were cured at 150 °C. The bulk resistivity of the hybrid ECAs with the decorated graphene were compared to those of conventional ECAs (epoxy-silver flakes) and hybrid ECAs with non-modified graphene (epoxy-silver flakes-non-modified graphene). Figure 7 shows the bulk resistivity of the samples cured at 150 °C. As can be seen in this figure, the resistivity of the hybrid ECAs with both decorated and non-modified graphene are less than that of the conventional ECAs for the both filler concentrations. The bulk resistivity of the hybrid ECA with the decorated graphene at 60 wt% of total silver content is 7.6×10^{-4} Ω cm, which shows 90 % reduction compared to the bulk resistivity of conventional

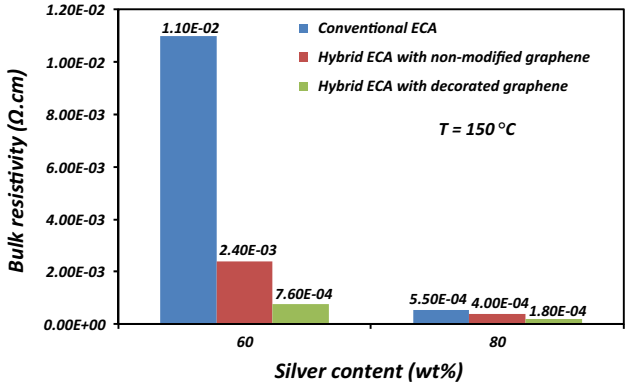

Fig. 7 The comparison between the electrical conductivity of conventional and hybrid ECAs at different filler concentrations of 60 and 80 wt% (for hybrid ECAs 1 wt% of nanofillers was used)

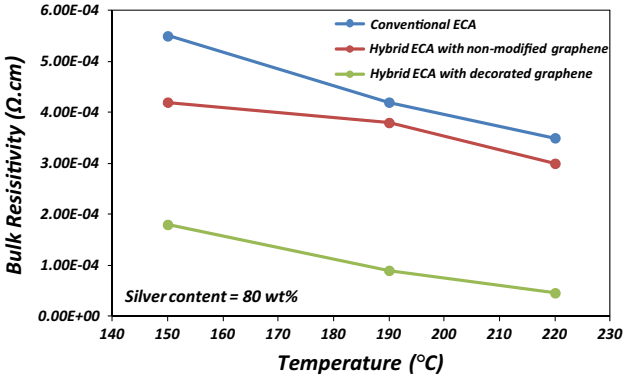

Fig. 8 The effect of curing temperature on the electrical conductivity of ECAs

ECA with the same filler content (1.1×10^{-2} Ω cm). This resistivity is close to that of the conventional ECA with 80 wt% of silver flakes. Also, the resistivity of the hybrid ECA with the decorated graphene at 80 wt% showed 67 % reduction compared to that of the conventional ECA with an equivalent silver content.

As electrons are transferred through the electrical pathways created by conductive fillers inside the ECAs, the morphology and quality of contact between fillers are crucial for the electrical conductivity of ECAs. The quality of contact between conductive fillers is related to the contact resistance which consists of a combination of constriction and tunneling resistances [35]. The constriction resistance represents the restriction of the free flow of electrons as they pass through a sharp contact point. The tunnelling resistance arises at the spot where there is no connection between fillers and electron tunnelling is required. The reduced electrical resistivity of the hybrid ECAs with both of non-modified and decorated graphene in comparison to that of conventional ECAs suggested that graphene nanosheets provide greater surface area than an equivalent amount of silver flakes for electron transportation within the network, which decreases the tunneling resistance, significantly. This situation is more pronounced at concentrations close to the percolation where the silver flakes are not fully in contact with each other.

To shed further light on the effect of Ag NPs on the electrical properties of the hybrid ECAs, the samples with 80 wt% of silver flakes were cured at different temperatures. The bulk resistivity data, shown in Fig. 8, revealed a much more significant resistivity reduction for the hybrid ECAs with the decorated graphene than for conventional ECAs and hybrid ECAs with non-modified graphene as curing temperature increased. A low bulk resistivity of 4.6×10^{-5} Ω cm was achieved for the hybrid ECAs with the decorated graphene cured at 220 °C, which is comparable to that of a typical eutectic solder (2×10^{-5} Ω cm) [3]. It demonstrates a great potential of this hybrid ECA as an alternative electrical interconnect material. These results suggest that the Ag NPs on the surface of graphene improve the electrical conductivity of conventional ECA at low curing temperatures, and their influence is more pronounced at higher curing temperatures. The presence of Ag NPs at low temperatures may increase the number of contact points in the filler system that in turn increase the contact resistance [5]. However, when the temperature increases they start to sinter to each other and to the flakes so as to provide direct metallurgical contacts between the silver flakes and graphene to form flake-NP-graphene-NP-flake conduction paths inside ECAs. This situation makes electron transportation more convenient through the electrical network and decreases the contact resistance among fillers.

4 Conclusions

We employed a simple room temperature wet chemistry approach to decorate graphene nanosheets with MPA-functionalized Ag NPs to be utilized as auxiliary fillers inside ECA nanocomposites and investigated the role of Ag NPs sintering on electrical conductivity of ECAs. The deposition of Ag NPs is based on the direct reduction of Ag ions adsorbed on the surface of graphene oxide using a strong reducing agent ($NaBH_4$) in the presence of MPA; NaBH4 was found to be able to reduce the graphene oxide back to graphene. FTIR, UV–Vis, XRD, and TEM confirmed the decoration of graphene with MPA-functionalized Ag NPs. The surface functionalization of Ag NPs made the decorated graphene dispersible in water and ethanol, and facilitated their dispersion in epoxy nanocomposite. TGA analysis of

the decorated graphene showed that the MPA start to decompose from the NPs surface at temperatures close to 150 °C. SEM images confirmed the sintering of Ag NPs at this temperature which resulted in significant reduction of bulk resistivity of the decorated graphene and silver flakes mixture "thin-film" at temperature higher that 150 °C. The addition of a small amount of the decorated graphene into the conventional ECA remarkably decreased its bulk resistivity, especially at concentrations within the percolation content. The bulk resistivity of hybrid ECAs with the decorated graphene significantly decreased as the curing temperature increased to 220 °C. A highly conductive ECA with a very low electrical resistivity of 4.6×10^{-5} Ω cm (close to that of eutectic solders) was achieved by incorporating a small amount of the Ag NP-decorated graphene (1 wt%) into the conventional ECAs (total silver content of 80 wt%). The high electrical conductivity of the fabricated ECA is attributed to the metallurgical connection between graphene and silver flakes inside the electrical network because of the sintering of small Ag NPs on the graphene surface.

Acknowledgments This work was supported by a Strategic Project Grant from the Natural Sciences and Engineering Research Council of Canada (NSERC).

References

1. Y. Li, K.S. Moon, C.P. Wong, Science **308**, 1419 (2005)
2. Y. Zhou, in *Microjoining and nanojoining (Ch. 17)*, vol. 1, ed. by S. Bohm, E. Stammen, G. Hemken, M. Wanger (CRC Press, Boca Raton, 2008)
3. C. Yang, C.P. Wong, M.M.F. Yuen, J. Mater. Chem. C. **1**, 4052 (2013)
4. W. Jeong, H. Nishikaw, D. Itou, T. Takemoto, Mater. Trans. **46**, 2276 (2005)
5. J. Jiang, K. Moon, Y. Li, C.P. Wong, Chem. Mater. **18**, 2969 (2006)
6. B.M. Amoli, S. Gumfekar, A. Hu, Y.N. Zhou, B. Zhao, J. Mater. Chem. **22**, 20048 (2012)
7. R. Zhang, K.S. Moon, W. Lin, C.P. Wong, J. Mater. Chem. **20**, 2018 (2010)
8. Z.X. Zhang, X.Y. Chen, F. Xiao, J. Adhes. Sci. Technol. **25**, 1465 (2011)
9. B. M. Amoli, E. Marzbanrad, A. Hu, Y. N. Zhou, B. Zhao 2013, Macromol. Mater. Eng. **299**, 739 (2014)
10. Y. Oh, K.Y. Chun, E. Lee, Y.J. Kim, S. Baik, J. Mater. Chem. **20**, 3579 (2010)
11. K.S. Novoselov, A.K. Geim, S.V. Morozov, D. Jiang, M.I. Katsnelson, I.V. Grigorieva, S.V. Dubonos, A.A. Firsov, Natrue **438**, 197 (2005)
12. V. Georgakilas, M. Otyepka, A.B. Bourlinos, V. Chandra, N. Kim, K.C. Kemp, P. Hobza, R. Zboril, K.S. Kim, Chem. Rev. **112**, 6156 (2012)
13. S. Stankovich, D.A. Dikin, G.H.B. Dommett, K.M. Kohlhaas, E.J. Zimney, E.A. Stach, R.D. Piner, S.B.T. Nguyen, R.S. Ruoff, Nature **442**, 282 (2006)
14. V.H. Luan, H.N. Tien, T.V. Cuong, B. Kong, J.S. Chung, E.J. Kima, S.H. Hur, J. Mater. Chem. **22**, 8649 (2012)
15. E.E. Tkalya, M. Ghislandi, G. With, C.E. Koning, Curr Opin Colloid Interface Sci **17**, 225 (2012)
16. K.P. Loh, Q. Bao, P.K. Ang, J. Yang, J. Mater. Chem. **20**, 2277 (2010)
17. Y. Jin, M. Jia, M. Zhang, Q. Wen, Appl. Surf. Sci. **264**, 787 (2013)
18. R. Pasricha, S. Gupta, A.K. Srivastava, Small **5**, 2253 (2009)
19. K. Liu, L. Liu, Y. Luo, D. Jia, J. Mater. Chem. **22**, 20342 (2012)
20. N.W. Pu, Y.Y. Peng, P.C. Wang, C.Y. Chen, J.N. Shi, Y.M. Liu, M.D. Ger, C.L. Chang, Carbon **67**, 449 (2014)
21. X. Peng, F. Tan, W. Wang, X. Qiu, F. Sun, X. Qiao, J. Chen, Mater. Electron. **25**, 1149 (2014)
22. K. Liu, S. Chen, Y. Luo, D. Jia, H. Gao, G. Hu, L. Liu, Compos. Sci. Technol. **94**, 1 (2014)
23. M.K. Singh, E. Titus, R. Krishna, R.R. Hawaldar, G. Goncalves, P.A.A.P. Marques, J. Gracio, J. Nanosci. Nanotechnol. **12**, 6731 (2012)
24. G. Goncalves, P.A.A.P. Marques, C.M. Granadeiro, H.I.S. Nogueira, M.K. Singh, J. Gracio, Chem. Mater. **21**, 4796 (2009)
25. J.I. Paredes, S. Villar-Rodil, A. Martinez-Alonso, J.M.D. Tascón, Langmuir **24**, 10560 (2008)
26. I.E. Dell'Erba, C.E. Hoppe, R.J.J. Williams, Langmuir **26**, 2042 (2010)
27. Y. Si, E.T. Samulski, Nano Lett. **8**, 1679 (2008)
28. B.A. Bourlinos, D. Gournis, D. Petridis, T. Szabó, A. Szeri, I. Dékány, Langmuir **19**, 6050 (2003)
29. A. Moores, F. Goettmann, New J. Chem. **30**, 1121 (2006)
30. E. Marzbanrad, A. Hu, B. Zhao, Y. Zhou, J. Phys. Chem. C **117**, 16665 (2013)
31. V.H. Pham, T.V. Cuong, S.H. Hur, E. Oh, E.J. Kim, E.W. Shin, J.S. Chung, J. Mater. Chem. **21**, 3371 (2011)
32. L. Zhou, H. Gu, C. Wang, J. Zhang, M. Lv, L. He, Colloid. Surf. A **430**, 103 (2013)
33. H.C. Schniepp, J.L. Li, M.J. McAllister, H. Sai, M. Herrera-Alonso, D.H. Adamson, R.K. Prud'homme, R. Car, D.A. Saville, I.A. Aksay, J. Phys. Chem. B **110**, 8535 (2006)
34. E. Cliffel, F.P. Zamborini, S.M. Gross, R.W. Murray, Langmuir **16**, 9699 (2000)
35. G.R. Ruschau, S. Yoshikawa, R.E. Newnham, J. Appl. Phys. **72**, 953 (1992)